Spatial structures of plasma filaments in the scrape-off layer on HL-2A

J. Cheng[1], L.W. Yan[1], J.Q. Dong[1], W.Y. Hong[1], K.J. Zhao[1], J. Qian[1], T. Lan[2], A D. Liu[2], D.F. Kong[2], Q.W.Yang[1], X. R. Duan[1] and Yong Liu[1]

[1]*Southwestern Institute of Physics, Chengdu, China*
[2]*Department of Modern Physics, University of Science and Technology of China, Hefei, China*
E-mail contact of main author: chengj@swip.ac.cn

Experimental results about plasma filament parallel coherence and three dimensional characteristics on the HL-2A tokamak are reported. Interchange mode with near-zero parallel wave number is found outside magnetic separatrix using the novel combination of a poloidal Langmuir 10-probe and a radial Langmuir 8-probe arrays toroidally separated by 210 cm. The ratio of poloidal to toroidal mode number is approximately equal to local safety factor for turbulent frequency below 100 kHz. Based on significant parallel coherence along a magnetic field line, filament propagation process is clearly observed in poloidal-radial plane. The suppression of turbulence power and filament radial velocity is studied during gas-puffing phase. In addition, filament generation mechanism is also discussed.

Keyword: Plasma filaments, parallel coherence, Langmuir probe array, interchange mode

1. Introduction

Spatial structures of plasma filaments (blobs) with relative high pressure to the bulk plasma locate in poloidal and radial plane and extend along the magnetic field line. These structures become significant sources for increasing cross-field transport in fusion devices. Filament-induced convective transport can increase particle recycling, reduce the divertor efficiency and lead to the high level erosion of the first wall [1-2]. Thus, filament three dimensional characteristics, parallel coherence and generation mechanism in scrape-off layer (SOL) are key issues in magnetically confined plasma. Theoretically, filaments were used as an initial condition and their propagation in the SOL was studied [3-5]. A self-consistent generation of filaments has been reported by *Russel* et al [6], but detailed three dimensional characteristics and generation mechanism have not been discussed yet. In toroidally confined plasma, filament spatial structures have been widely observed using fast cameras and Langmuir probe diagnostics [7-12]. More investigation of filaments is aimed at their statistical properties in radial or poloidal direction. For example on JT-60U, the comparison of fluctuation characteristics at low and high field sides indicated that filaments are easier to form at the low field side [13]. On TCV, experimental result shows a good agreement between filament characteristics measured with reciprocating probes and simulation of two-dimensional interchange turbulence code [14]. There are some experimental results for identifying filament generation mechanism. On the TORPEX device with open magnetic field lines, interchange mode dominates filament formation [15]. On the TJ-K, drift wave turbulence is probably responsible for filament generation when magnetic field line transition

from close to open [16]. Filaments had been also widely observed in linear devices without magnetic field curvature, such as VINETA. They are reported forming from quasi-coherent drift wave with m = 1 mode [17]. Up now, filament parallel coherence, spatial birth zone and generation mechanism have not been unambiguously identified on tokamaks, which are still open issues. Understanding filament parallel correlation characteristics and generation mechanism is critical to look effective methods reducing edge cross-field transport. Therefore, our focus is put on the simultaneous measurement of filament three-dimension characteristics based on the significant parallel correlation along a magnetic field line.

In this paper, we study filament parallel coherence and three dimensional spatial characteristics with the novel combination of a poloidal 10-probe array and a radial 8-probe array, which are toroidally separated by 210 cm. The dependence of filament parallel coherence along a magnetic field line on different poloidal positions is obtained by changing pitch angle. The ratio of poloidal to toriodal mode number is close to local safety factor q for the turbulent frequency below 100 kHz. Two isolated filaments continuously moving in poloidal-radial plane is clearly observed according to significant parallel coherence. In addition, radial electric field and filament radial velocity are strongly suppressed during gas-puffing.

2. Experimental setup

Plasma filament experiments were performed in ohmically heated deuterium discharges on the HL-2A tokamak with major radius $R = 1.65$ m and minor radius $a = 0.4$ m [18]. Typical experimental parameters were plasma current $I_p = 168$ kA, toroidal magnetic field $B_t = 1.9$ T, line-averaged density $n_e = 1.9 \times 10^{19}$ m^{-3}. The Greenwald density limit was $n_G = 3.3 \times 10^{19}$ m^{-3}. Three dimensional characteristics of zonal flows and geodesic acoustic mode were identified on the HL-2A tokamak with Langmuir probe arrays [19-20]. The statistical characteristics of blob turbulence across the separatrix had been studied with 5-tip Langmuir probe array in HL-2A edge plasma [21]. Recently, two novel Langmuir probe arrays are combined to investigate three dimensional characteristics of plasma filaments, as shown in figure 1. One is a poloidal 10-tip array (labeled as 'Array A') locating below the midplane. The distance between the first probe and midplane is $d_1 = 2.1$ cm, the separation between the first tip and the ith tip in array A is defined as $\Delta d_\theta (i) = (i-1)\Delta d$ ($1 \leq i \leq 10$), where Δd = 4 mm is the adjacent probe separation. The maximum radial distance between a tip and the same magnetic flux is below 4.0 mm, which is
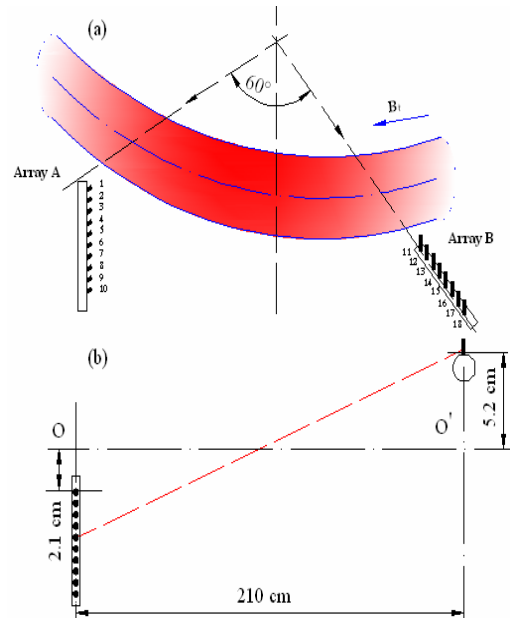

FIG. 1. The combination of poloidal and radial probe arrays with toroidally spaced by 60 degree. Adjacent separation of two tips in array A and array B is 4 mm.

comparable with the exposed probe length. Another is a radial 8-tip array (labeled as 'Array B'), which is positioned at $d_2 = 5.2$ cm above the mid-plane. The toroidal separation between probe arrays is 210 cm, which is large enough for toroidally spatial resolution. Langmuir probes are used to measure the floating potentials or ion saturation current with negative biased voltage ~160 V. This probe array arrangement provides enough flexibility to study filament dynamics and propagation characteristics, especially, the parallel coherence along a magnetic field line. Data are acquired with frequency $f_s = 1$ MHz and accuracy of 12 bits.

3. Experimental results

3.1. Identification of near-zero parallel wave numbers

The measurement of parallel wave number ($k_{//}$) is important to distinguish the interchange mode and drift wave based on their unique $k_{//}$. The former with $k_{//} = 0$ propagates across a field line, while the latter moves obliquely to a field line with small $k_{//} \neq 0$. Thus, the $k_{//}$ accurate measurement is critical for identifying instability mechanism. In principle, the parallel wave number can be estimated with the phase shift between Langmuir probes, which is measured in the SOL of HL-2A plasma. For suitable B_t and I_p, a field line passing one tip of the array B may intersect the ith tip in the array A at the vertical position $z_0 = (i-1) \Delta d + d_1$, which is defined as the distance between the mid-plane and the intersection. The z_0 needs satisfy this condition: $((z_0+d_2)/L_\phi) = 2 \times 10^{-7} I_p/(a+\Delta r)B_t$, where L_ϕ denotes the toroidal separation between array A and array B, Δr is radial distance between a tip in array A and the magnetic separatrix. Positive Δr means outside the separatrix. Figure 2 (a) shows the contour plot of the maximum correlation between tips in array A and array B. The peak of maximum correlation appears at the $\Delta r \sim 16$ mm and $\Delta d_\theta \sim 16$ mm, which is close to an ideal field line intersection at the array A, locating at $z_0 = 3.7$ cm (i~5) estimated with the discharge parameters $I_p = 168$ kA and $B_t = 1.9$ T. This result implies the 5th tip in array A and the 15th tip in array B close to the same field line. Thus, the maximum coherence and the wave number k between any tip in array A and the 15th tip in
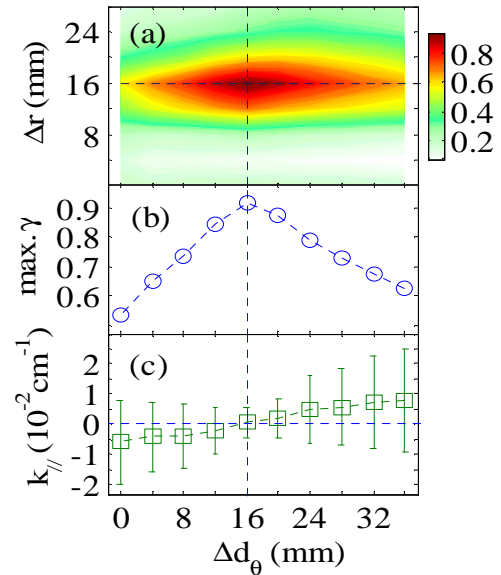

FIG.2. The contour plot of maximum cross correlation between arrays (a), the maximum correlation (b) and averaged parallel wave number (c) between each tip in array A and a fixed tip in array B.

array B can be calculated. The average wave number $<k>$ and its width σ_k have been evaluated using two-point correlation spectrum $S(k, f)$ [22], i.e., $k = <k> \pm \sigma_k$. Figure 2(b) and 2(c) show their maximum correlation and averaged wave number versus poloidal distance Δd_θ. The error bars represent the full width at half magnitude (FWHM) of spectrum $s(k)$. The maximum coherency 0.91 appears at the $\Delta d_\theta = 16$ mm, where the parallel wave number change

its sign, marked by the vertical dotted line. This observation is consistent with the interchange mode characteristics with near-zero parallel wave number.

3.2 Joint spectrum characteristics in the SOL

Inside the separatrix about 2.0 cm, three-dimensional spectral characteristics of zonal flows and GAM had been studied in detail [23-25]. In this part, our focus is put on the spectral characteristics of SOL plasma. The maximum coherence between the 5th tip in array A and the 15th tip in array B is over 0.9 and the phase shift remains close zero below 100 kHz. Based on this significant parallel coherence, the joint spectrum $s(k_{//}, k_\theta)$ and $s(k_r, k_\theta)$ are estimated for the frequency below 100 kHz. The poloidal wave number k_θ is calculated with the 6th tip in array A and the 15th tip in array B, while the radial wave number k_r is estimated with the 5th tip in array A and the 16th tip in array B. This choice is to remove small-scale structures with short parallel coherence length. Thus, the joint spectrum mainly shows the contribution of spatial structures with significant long-range correlation. In figure 3(a), there is a noticeable peak appearing at the nonzero poloidal wave number and close zero parallel wave number. The averaged poloidal and parallel wave number are estimated to be $k_\theta = 1.2 \pm 0.7$ cm^{-1} and $k_{//} = 1.9 \times 10^{-3} \pm 2.5 \times 10^{-3}$ cm^{-1}, respectively. The poloidal and parallel length are calculated to
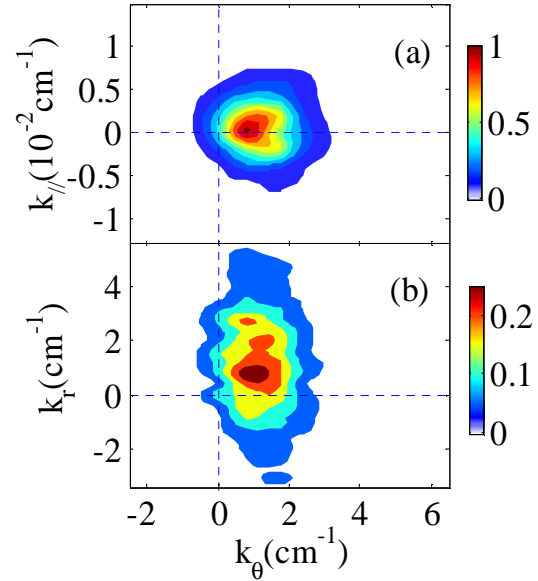

FIG.3. The joint spectrum of poloidal-parallel wave number (a) and the poloidal-radial wave number (b) This estimation is based on the significant parallel correlation between tips lying in the same field line.

be $L_\theta \sim 2.6$ cm and $L_{//} \sim 16.5$ m, respectively. This estimation shows that filament extends at least once around the torus during filament lifetime (typical lifetime $\tau_c = 20$-30 μs). The measured parallel propagation velocity is about $V_{//} = L_{//}/\tau_c \sim (6.0$-$8.3) \times 10^5$ m/s, which is between the ion sound speed $C_s \sim 4.3 \times 10^4$ m/s and electron thermal speed $V_{th,e} \sim 1.3 \times 10^6$ m/s. This result is similar to that measured on the JET [26]. Figure 3(b) shows the joint spectrum $s(k_r, k_\theta)$ in wave number space. The power peak has the nonzero radial and poloidal wave numbers. The spectral asymmetry implies non-zero Reynolds stress $\langle v_r v_\theta \rangle$, which is proportional to the weighted average $\Sigma k_r k_\theta |\phi|^2$. The averaged radial wave number and its FWHM are estimated as 1.3 cm^{-1} and 1.4 cm^{-1}, respectively. This observation suggests that radial decay of spatial structure is the fastest among radial, poloidal and parallel directions.

3.3. Parallel coherence dependent on poloidal position

The significant parallel coherence along a field line has been observed under a fixed pitch

angle. It is also scanned with different pitch angles. Based on the significant parallel coherence of two probes in the same field line, the local safety factor q can be estimated using $q = a/(R\theta)$, where the pitch angle θ is calculated by the probe geometric position with maximum correlation. Array A is localized at near SOL, e.g., $\Delta r = 5$ mm. Figure 4(a) shows that plasma current continuously increases from 136 kA to 194 kA within 1050 ms in shot 13500, while the toroidal magnetic field is fixed at $B_t = 1.9$ T. Figure 4(b) shows the dependence of significant parallel coherence on the different poloidal positions in array A. This result suggests that a field line intersection point shifts from the first tip to the 10th tip in the array A when plasma current rising, whose rising rate is estimated as 0.06 kA/ms. The scanned poloidal distance passing by a field line is calculated as 0.33 cm within 100 ms, which is below the adjacent probe separation of 0.4 cm. Therefore, the change of magnetic field pitch angle can be neglected within 100 ms. Here, the chosen discharge parameters are $I_p \sim 168 \pm 2.5$ kA and

FIG.4. The temporal evolution of plasma current (a) and the contour plot of maximum correlation between each tip in array A and the 15th tip in array B (b). The poloidal mode number m (c), torioidal mode number n (d) and their ratio m/n (e) measured from 950ms to 1050ms, as indicated by two vertical dotted lines.

$B_t = 1.9$ T from 950 to 1050 ms, indicated by two vertical dot lines in figure 4 (a) and figure 4 (b) for studying mode characteristics. During this time, local safety factor q is estimated as 5.5~5.7. The parallel, toroidal and poloidal wave number should meet the vector rule, e.g., $k_{//}=k_\phi \cos\theta + k_\theta \sin\theta$. Then, the poloidal mode number m and toroidal mode number n are estimated using $m = k_\theta(a+\Delta r)$ and $n = k_\phi(R+a+\Delta r)$, respectively. As shown in figure 4(c) and figure 4(d), poloidal and toroidal mode numbers are invariant below 10 kHz. In 10-100 kHz, they increase from 10 to 40 and 2 to 8, respectively. But in this frequency range, the ratio of the former to the latter remains constant 5.5, which is close to local safety factor q, see figure 4(e). Over 100 kHz, the poloidal and toroidal mode numbers become random. This observation indicates the significant parallel coherence existence when two probes locating at the same field line.
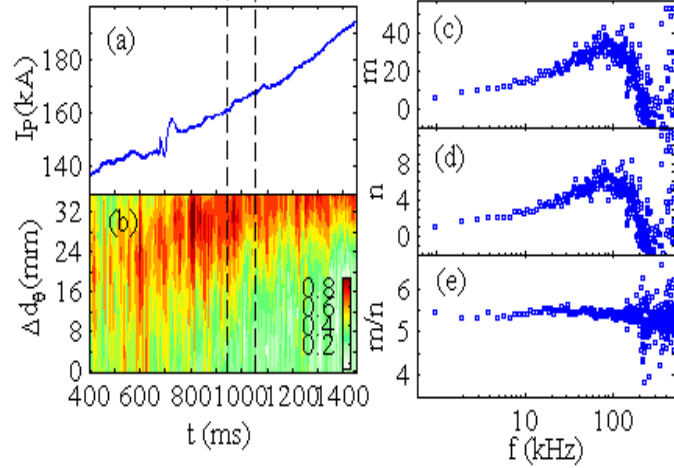
3.4. Filament propagation in SOL

Based on the significant parallel correlation described in the part 3.1, spatial structures in poloidal-radial plane (2D) have been clearly observed using the novel combination of a poloidal and a radial probe arrays. Cross-conditional average [27] is used to extract spatial structures from ambient turbulence based on a given amplitude threshold. There are two isolated filaments appearing in 2D plane outside the separatrix. The first filament (marked by a circle) appears with poloidal and radial sizes less than 10 mm, see figure 5 (a), and then its

amplitude gradually grows, as shown in figure 5(b) and figure 5(c). Meantime, the second filament moves into our observation region (denoted by a cross), see figure 5(d), which has a separation of 25 mm from the first one, indicating that they are independent filaments. These

structures probably form inside the separatrix and then propagate across the separatrix into the SOL. Figure 5(e) illustrates that the second filament gradually moves into our measurement region, and the distance between them becomes smaller, indicating that the second filament moves faster than the first one. As shown in figure 5(f), the first filament almost disappears, which suggests that the filament lifetime is about 20-30 µs. From figure 5(f) to figure 5(h), the poloidal movement of the second filament is apparent, but its
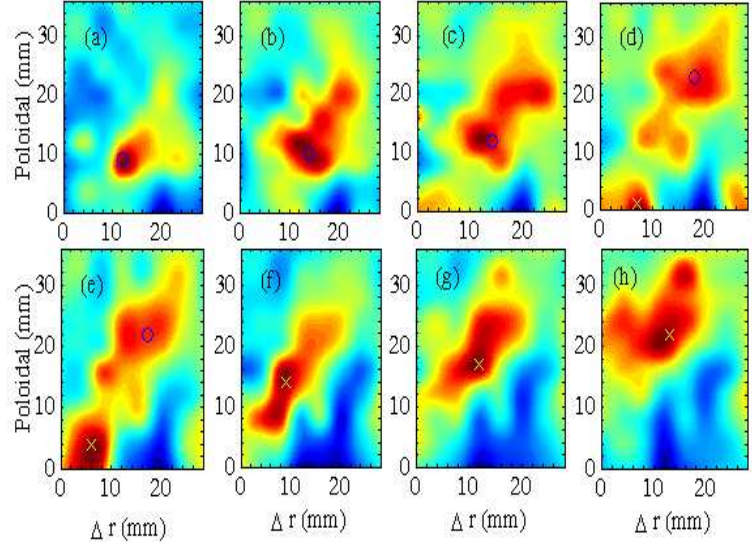

FIG.5. The 2D images of conditional average of floating potentials measured with poloidal 10-probe and radial 8-probe arrays at 8 different delay times.
The adjacent interval is 5 µs.

radial movement is ambiguous, which implies the faster poloidal movement than the radial movement. According to results in W-7 AS stellarator [28], it seems to be more reliable to calculate filament velocity with 2D correlation image than that with purely poloidal or radial probe arrays. Therefore, in this observation region, filament radial and poloidal velocities are estimated to be about 0.5-0.9 km/s and 1.1-2.0 km/s, respectively, using $V = \Delta x/\Delta t$, where Δx is the movement distance in 2D plane during the interval Δt. The filament radial velocity is about 2 % of ion sound speed C_s. In addition, the most obvious feature is filaments inclination in the 2D plane, which may be correlation with the radial magnetic shear.

3.5. Filament radial movement suppressed by gas-puffing

Filament radial velocity is a key parameter for cross-field transport. Thus, in this part we focus on the study of filament radial propagation and turbulent spectrum characteristics during gas-puffing. Figure 6(a) shows the temporal evolutions of modulated gas-puffing pulses with a width about 80 ms and an interval about 120 ms. The plasma horizontal displacement is less than 4 mm during gas-puffing phase, which is comparable with probe adjacent interval. The contour plot of radial electric field shows that most power is localized below 40 kHz, see figure 6(b). Figure 6(c) shows the contour plot of turbulent spectrum width σ_k, which is reverse proportional to correlation length. Filament radial velocity near the separatrix is estimated with cross-conditional average between E_θ/B_t and n_e, as shown in figure 6(d). The peak of cross-condition average at the time deviated from maximum density $\Delta\tau = 0$ means filament radial velocity [21]. It is clearly seen that radial electric field is

strongly suppressed during gas-puffing. Meanwhile, turbulence correlation length is shortened. It is interesting to note that filament radial velocities also reduce when gas-puffing switching on. This observation implies the filament generation or its movement strongly influenced by plasma edge parameters. In a recent theoretical study [29], *Bisai et al* have found some edge parameters impacting on the growth rate of interchange mode, such as temperature and density gradients. The former is proportional to mean radial electric field and is more easily to trigger interchange mode to grow than the latter. Our experimental observation is roughly consistent with the theoretical prediction. Detail results will be presented in another paper.
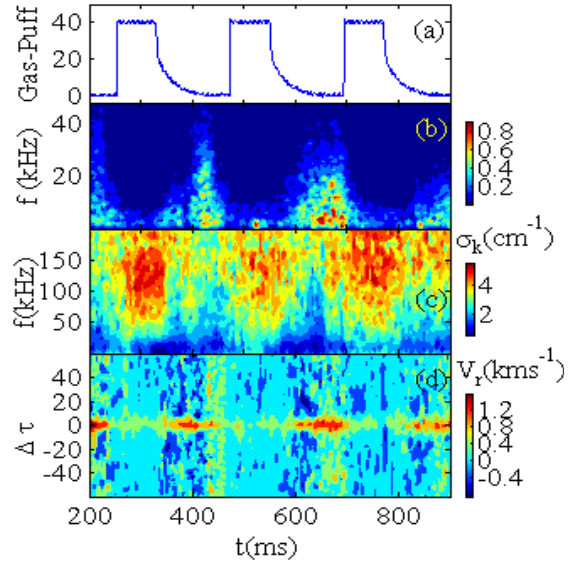
FIG. 6. *Temporal evolution of modulation gas puffing (a), the contour plot of radial electric field (b), spectrum width (c) and filament radial velocity (d).*
Measured position is near separatrix.

4. Summary

Significant parallel correlation and three-dimensional characteristics of plasma filaments in the SOL plasma of HL-2A tokamak are studied using a novel combination of a poloidal Langmuir 10-probe and a radial 8-probe arrays toroidally separated by 210 cm. Near-zero parallel wave number is observed outside the separatrix. The ratio of poloidal to toriodal mode numbers is close to local safety factor for the turbulent frequency below 100 kHz. Based on significant parallel coherence, the propagation processes of two isolated filaments in poloidal-radial plane are clearly observed. This result implies that filaments form inside the separatrix. The filament lifetime is about 20-30 μs. Typical radial and poloidal velocities are about 0.5-0.9 km/s and 1.1-2.0 km/s, respectively. Additionally, the radially electric field and filament movement velocity can be strongly suppressed by gas puffing, which indicates that there is a possible link between the interchange mode and filament generation mechanism.

Acknowledgments

References

[1] Krasheninnikov S.I., Phys. Lett. A. **283** (2001) 368
[2] Zweben S.J., et al Plasma Phys. Control Fusion **49** (2007) S1
[3] D'Ippolito D.A., et al Phys. Plasmas **9** (2002) 222
[4] Garcia O.E., et al Phys. Rev. Lett. **92** (2004) 165003
[5] Aydemir A.Y., et al Phys. Plasmas **12** (2005) 062503
[6] Russell D.A., et al Phys. Rev. Lett. **93** (2004) 265001
[7] Grulke O., et al Phys. Plasmas **8** (2001) 5171
[8] Terry J.L., et al Phys. Plasmas **10** (2003) 1739
[9] Boedo J.A., et al Phys. Plasmas **10** (2003) 1670
[10] Devynck P., et al Phys. Plasmas **13** (2006) 102505
[11] Myra J.R., et al Phys. Plasmas **13** (2006) 092509
[12] Agostini M et al Phys. Plasmas **14** (2007)102305
[13] Tanaka H., et al Nucl. Fusion **49** (2009) 065017
[14] Garcia O.E., et al, Plasma Phys. Control. Fusion **48** (2006) L1
[15] Furno I., et al Phys. Rev. Lett. **150** (2008) 055004
[16] Happel T., et al Phys. Rev. Lett. **102** (2009) 255001
[17] Windisch T., et al Phys. Plasmas **13** (2006) 122303
[18] Duan X.R., et al Nucl. Fusion **49** (2009) 104012
[19] Zhao K.J., et al Phys. Rev. Lett. **96** (2006) 255004
[20] Liu A.D., et al Phys. Rev. Lett. **103** (2009) 095002
[21] Cheng J., et al Plasma Phys. Control Fusion **52** (2010) 055003
[22] Beall J.M., et al J. Appl. Phys. **53** (1982) 3933
[23] Yan L.W., et al Nucl. Fusion, **47** (2007) 1673
[24] Lan T., et al Phys. Plasmas **15** (2008) 056105
[25] Cheng J., et al Nucl. Fusion **49** (2009) 085030
[26] Thomsen H., et al Phys. Plasmas **9** (2002) 1233
[27] Pecseli H.L. and Trulsen J., Phys. Fluids B **1** (1989) 1616
[28] Bleuel J., et al New J. Phys. **4** (2002) 38
[29] Bisai N., et al Phys. Plasmas **11** (2004) 4018